6 Monte Carlo Studies of Detector Performance

This chapter describes the Monte Carlo studies that were carried out to optimize the detector design and quantify the important performance characteristics of the detector, including vertex and tracking resolution, particle identification, and energy resolutions.

6.1 Detector Simulation

Simulation of neutrino interactions in MINERνA is carried out by a GEANT3-based Monte Carlo program. This program combines a flexible description of the detector geometry, the NuMI neutrino beam flux from the beam simulation, neutrino interaction physics from either of the two generators and simulation of the scintillator response with the standard tracking and particle interaction routines available in GEANT.

6.1.1 GNuMI flux interface

The output of the GNuMI simulation of the beamline is a set of files recording the neutrino flux in 0.5 GeV bins for a nominal number of protons on target. The flux files are in a standard format and hence can be interchanged with no additional modifications to the code. In this way different beam configurations can be easily studied. An option exists to generate interactions with a flat energy spectrum. In this case, beam weights are stored in an output ntuple. This is particularly useful if one wishes to study the effect of different beam configurations without furthur Monte Carlo running.

6.1.2 Event generator interface

The Monte Carlo simulation program can be configured to accept neutrino interactions from either NEUGEN3 or NUANCE. The results of a neutrino interaction can be passed to the simulation in a number of ways. By default, the event generation routines in NEUGEN3 are usually called from within the simulation itself. In this mode, the code chooses a neutrino energy from the flux files, samples the density of material along the neutrino path; chooses a vertex and nucleus type, calls the kinematics generator and inserts the list of particles thus obtained into the GEANT data structures. This is not the only mode of generation. As a stand-alone generator, NUANCE provides events in either a text or ntuple format and so a provision is made to read in events from a standard external format. NEUGEN3 has been modified to write out events in the same format, so that the results of both generators may be compared in a consistent manner.

6.1.3 Geometry

Flexibility drives the design of the detector geometry code. The size, segmentation, material and shape of all components of the detector can be set and altered almost entirely from input datacards. The detector is logically divided into longitudinal sections. Each section can have different dimensions, strip sizes and absorber widths. In addition the absorbers in each section can be be constructed from segments of differing material and widths. The geometry description is sufficiently abstract that

minor changes in detector design may be accommodated merely by changing the datacard, allowing for fast detector reconfiguration and easy bookkeeping.

6.1.4 Hits and digitizations

Particles are tracked through the GEANT geometry in the standard manner. When a particle traverses a sensitive detector volume the particle type, volume identifier, entrance and exit points and energy deposition (including Landau and other fluctuations) are recorded as a hit. When GEANT has finished tracking the event, the hits are considered and converted to digitizations. There are as many digitizations as there are strips hit. Multiple hits on a single strip are condensed into one digitization, although information on which tracks contributed to the digitization is stored. These digitizations are then passed to the event reconstruction program.

6.1.5 Detector response and calibration simulation

The GEANT detector simulation assumes "ideal" light collection, and records the raw energy deposited in each channel. During event reconstruction, the energy deposited is converted to a number of detected photo-electrons. The scale factor between energy deposited and expected photo-electrons detected is determined by a standalone optical simulation validated for MINOS (see Section 6.2): the expected number of photo-electrons is smeared by Poisson statistics, and a 10% channel-to-channel Gaussian smearing reflecting a conservative estimate of remaining systematics after calibration and attenuation corrections.

6.2 Light Yield Simulation

In addition to the GEANT-3 based detector Monte Carlo, a standalone photon transport Monte Carlo was used to estimate the light yield of the proposed design. The photon transport Monte Carlo (LITEYLDX) was originally written by Keith Ruddick [174] and was modified to simulate the triangular extrusions of MINERνA. It was tuned to reproduce the known characteristics of the MINOS scintillator, namely that the average light yield from a MINOS module is 4.25 photo-electrons/MIP at a distance of 4 meters, and attenuation in the fiber is well described in terms of a double exponential: [175]:

$$N(x) = A(\exp(-x/90\mathrm{cm}) + \exp(-x/700\mathrm{cm})). \tag{1}$$

Particle identification studies described in Section 6.3.5 indicate that for a triangular extrusion, average light levels above 3.9 photo-electrons/MeV are required from a MIP in the inner detector. Coordinate resolution, vertex finding, and track pointing are affected by light levels to a lesser extent. Measurements in the vertical slice test indicate that actual light level in the inner tracker, including transmission and connector losses, will be 4.7 PE/MeV.

The photon transport Monte Carlo was used to calculate, for a given 'configuration' (strip geometry, fiber diameter, and fiber placement), the number of photons trapped in the fiber for a MIP entering at a particular position. This information is then used to determine a relative light collection efficiency for a particular configuration compared to MINOS strips. With the overall normalization
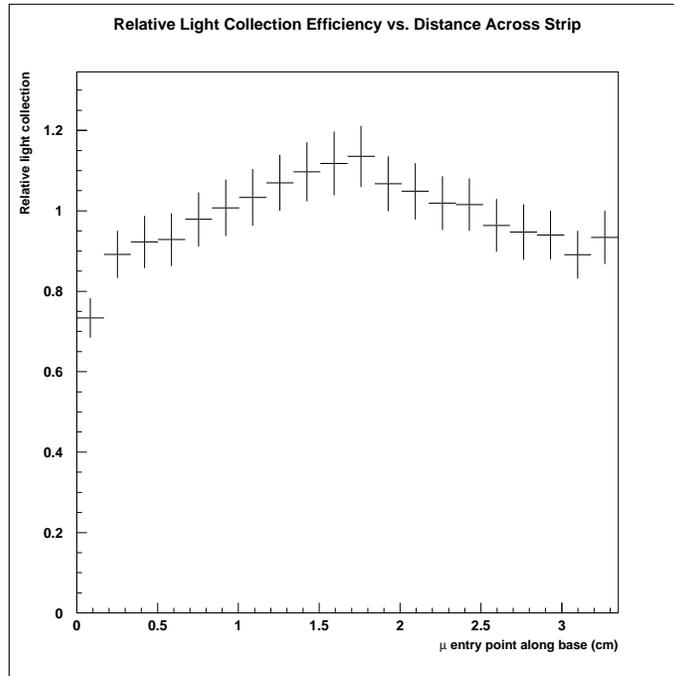
Figure 1: Relative light collection efficiency for a MIP crossing at normal incidence along the base of the scintillator extrusion.

and attenuation curve from MINOS one can then calculate the amount of light for any particular configuration. Figure 1 shows the relative light collection efficiency for a triangular extrusion where the entry point of the minimum ionizing particle is varied across the strip width, and indicates that the collection efficiency varies by $\pm 10\%$ over the strip width.

The overall light levels from 3 lengths of strips are shown in Figure 2. Here we have assumed a 90% reflectivity from the mirror end of the strip, and in all cases a 1 meter WLS 'pigtail' from the end of the near end of the strip to the PMT face. Clear fiber lengths and connectors are not included. Shown are the light levels predicted for 3 strip lengths. In each plot, the lowest curve corresponds to light collected from reflections off the mirrored end, the middle line corresponds to light travelling directly from the MIP to the readout end, and the upper line is the sum. As the figure shows, the light level in the inner tracking detector, with a maximum length of 2.2 m, meets the design requirement of 7.8 PE/MIP over the entire length.

6.3   Event Reconstruction

The output of the detector simulation is a list of digitizations for each strip. We have developed a basic reconstruction program which takes this list and reconstructs the tracks and vertices in an event.
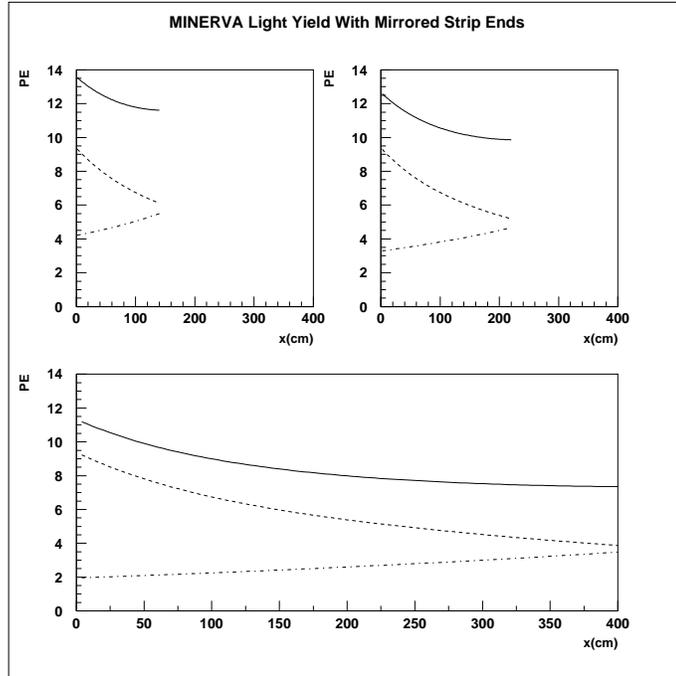
MINERVA Light Yield With Mirrored Strip Ends

Figure 2: Light yield vs. distance along strip for MINERνA scintillator strips with one-ended readout with a mirrored end. Dot-dashed line is light collected from reflections off the mirrored end, dashed line is light travelling directly to the readout end; solid line is the sum.

6.3.1 Pattern recognition

For our design studies, we have adopted "omniscient" pattern recognition based on Monte Carlo truth information. All hits generated by a given track (ignoring channels with overlap) are used to reconstruct the track. Development of a fully-realistic pattern-recognition algorithm to associate hits to track candidates has not been undertaken as yet due to manpower and time constraints. We are confident that the three-dimensional XUXV modular design of the detector, and its relatively modest occupancy, will allow highly-efficient pattern recognition and track identification. Visual inspection of events through the graphical interface of the detector simulation program reinforces this conclusion.

6.3.2 Coordinate reconstruction

Tracks generating hits in at least six scintillator planes of the inner detector, including three planes of the X view, can be reconstructed. Coordinates are estimated from the raw, smeared digitizations, using only planes which have one or two strips hit. Tracks at high angles to the detector axis may pass through more than two strips in a single plane, and it should be possible to recover these higher-multiplicity hits with a more sophisticated algorithm. For single hits, the coordinate is taken as the center of the strip. For dual hits, the position is interpolated using the charge-sharing between between strips, with a small geometrical correction based on the estimated crossing angle.

The coordinate resolution for a large test sample of single and double hits can be measured directly using the residuals obtained when each coordinate is excluded, in turn, from the track's fit. This coordinate resolution is parameterized as a function of the track's crossing angle, and used to assign errors to coordinates in the fitter.

6.3.3 Track finding

Reconstructed coordinates are used to fit each track using a Kalman filter algorithm[177]. For this proposal, tracking performance has only been studied in the non-magnetic region of the detector; the track model is perforce a strictly linear one. Neglect of the magnetic field is justified because mission-critical resolutions are determined by performance of the fully-active (non-magnetized) volume, and since coordinate resolution for the strips should not depend on the presence of a magnetic field. The momentum resolution for charged tracks in a magnetic field can be reliably estimated from the coordinate resolution, momentum and field strength. As long tracks may pass through many radiation lengths of scintillator and absorbing material, the Kalman filter's ability to correctly account for multiple Coulomb scattering ("process noise") is essential. The algorithm can optionally be used to exclude outliers from the fit.

Figure 3 shows the expected hit residuals, impact parameter and angular resolution for muons from a sample of quasi-elastic interactions, assuming triangular strips of 3 cm width and 1.5 cm thickness (close to the final design values). Hit resolutions of ~ 3 mm and angular resolutions of $< 0.5°$ are expected. These are consistent with the measurements made in the Vertical Slice Test which indicated a coordinate resolution of 3.2 mm. The coordinate resolution is degraded to approximately 1.5 cm if rectangular strips are employed instead of triangular ones, since interpolation based on charge is no longer possible.

6.3.4 Vertex finding

In this study, reconstructed tracks are associated to vertices using Monte Carlo truth information. The vertex positions are then fit using a Kalman filter algorithm. Track directions at the vertex are updated taking account of the constraint. This is equivalent to a least squares fit, but mathematically more tractable since it does not involve inversion of large matrices and can be easily extended to a helical track model. The primary vertex resolution for a sample of simulated quasi-elastic interactions with two visible tracks is shown in Figure 4. The transverse (longitudinal) vertex postion can be measured to a precision of better than (slightly more than) a centimeter.

6.3.5 Particle identification

Particle identification in MINERνA will rely on measuring specific energy loss (dE/dx) as well as topology (hadron and electromagnetic showers, decay signatures).

Electromagnetic showers   Electromagnetic showers are easily identifiable by their diffuse track and characteristic dE/dx profile in the fully-active central detector and energy deposition in the electromagnetic calorimeters. In addition, the fine granularity of MINERνA allows us to distinguish
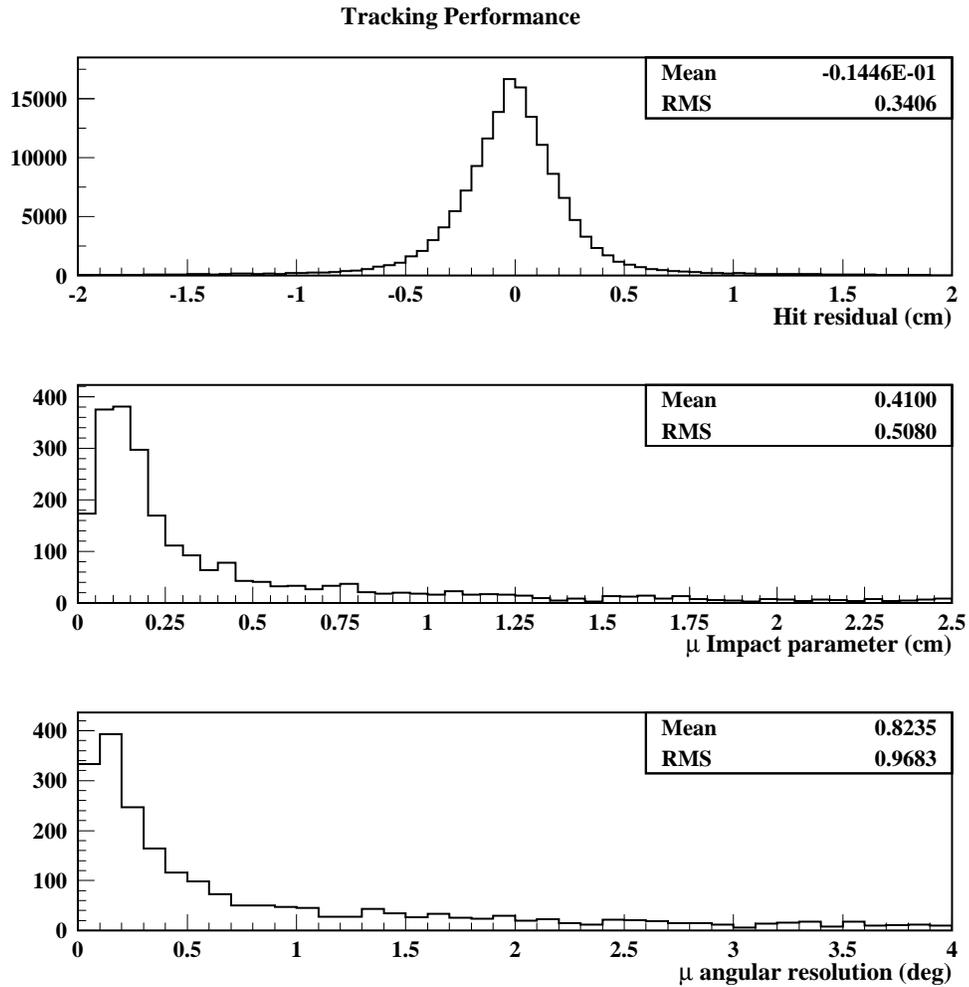
Tracking Performance

Figure 3: Performance of the tracking algorithm on muons from from a sample of simulated charged-current quasi-elastic interactions. Shown are (top) the hit residuals, (middle) the impact parameter of the muon with the vertex and (bottom) the muon angular resolution.
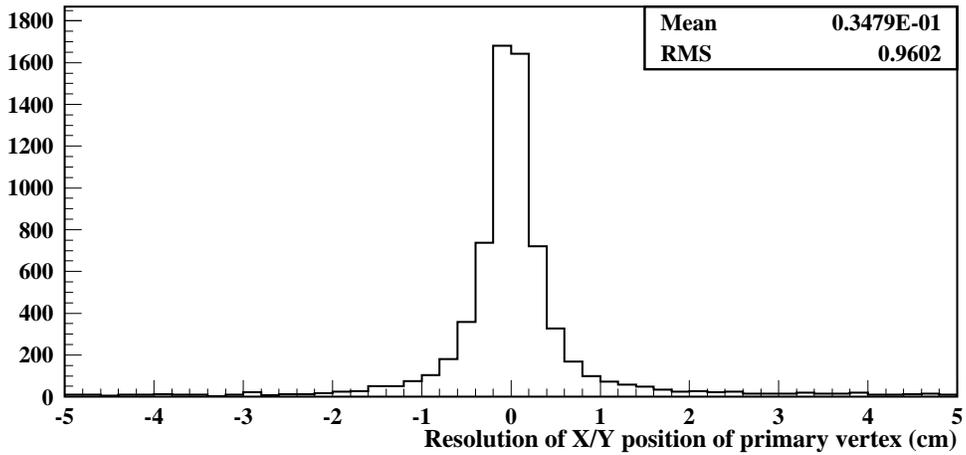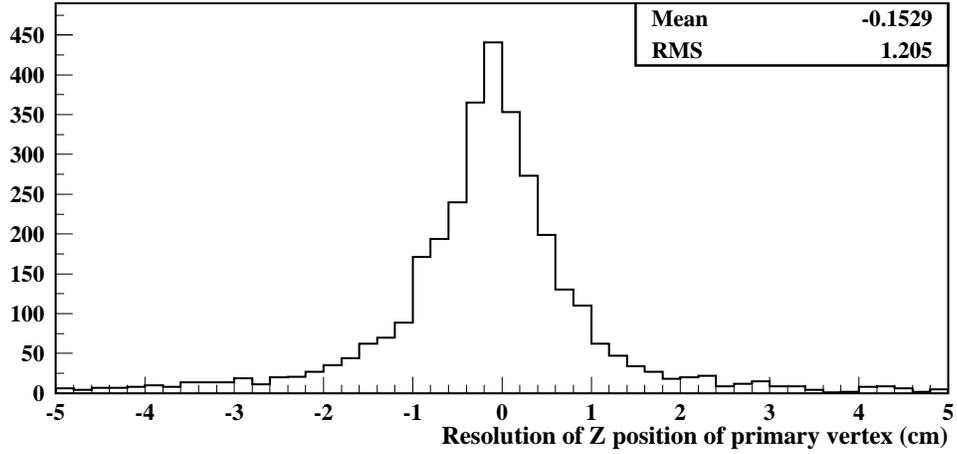
Figure 4: Reconstructed vertex resolution for two track charged current quasielastic events. Shown are (top) the resolution in the longitudinal position of the vertex (Z) and (bottom) the resolution of the transverse position of the vertex (X and Y).

electrons and photons, when the primary vertex is known, using distance to shower onset and shower length. Figure 5 shows the distance between the electromagnetic shower origin and the true primary vertex for charged-current ν_e interactions and π^0 production. The figure also shows the length of the showers, measured in MINERνA scintillator planes, or 1.75 cm of polystyrene. For neutral pions the length is from the beginning of the first showering photon to the end of the second one.
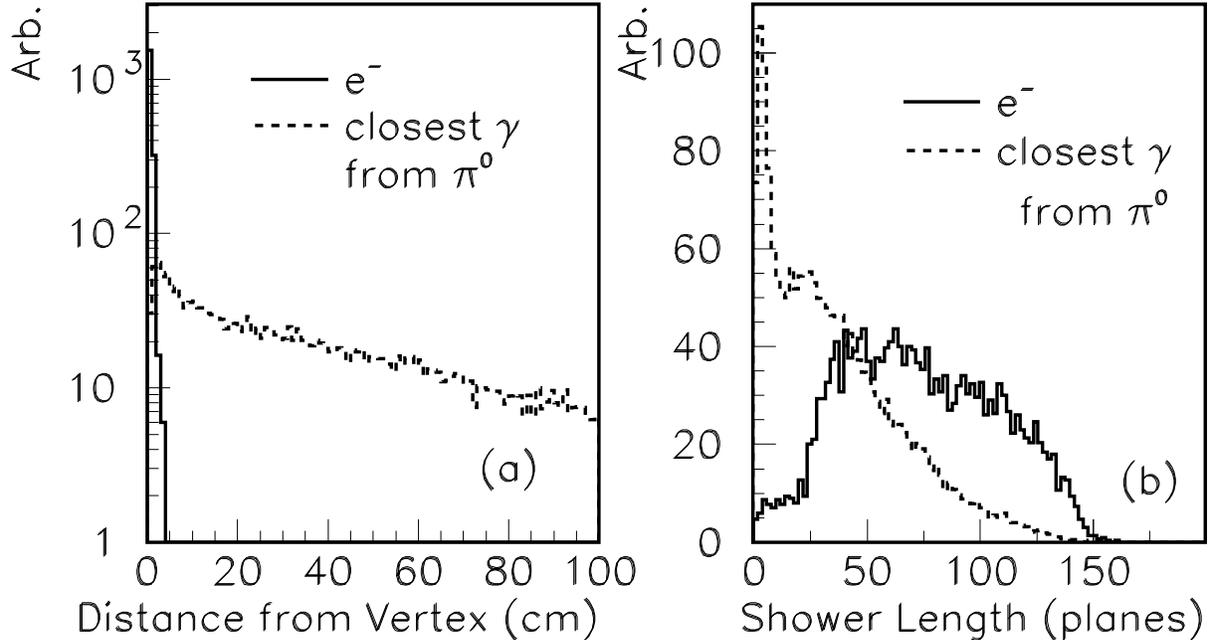

Figure 5: (a) The distance in centimeters between the neutrino vertex, which can be determined from a proton track, and the start of the most upstream electromagnetic shower, for both electrons and photons from neutral pions. (b) The shower length in units of scintillator planes, for electrons and neutral pions.

Electromagnetic energy resolution The energy resolution of the detector has been determined with Monte Carlo simulations using single electrons. The dependence of the resolution on the electron energy, angle, and track length in the inner detector have been determined. For forwardgoing electrons at the front of the inner detector the energy dependence is shown in Figure 6. The energy resolution for this situation can be parametrized as

$$\sigma/E = 1.0\%/\sqrt{E} + 2.7\%. \tag{2}$$

The calorimetric capabilities of the detector for low energy showers are quite strong, for example the energy resolution for these 1 GeV electrons is = 3.7%. Figure 7 shows the energy resolution for 1 GeV electrons as a function of the electron angle. Electrons at less than 20° to the beam direction strike the downstream ECAL while those with $\theta > 20°$ hit the barrel ECAL.
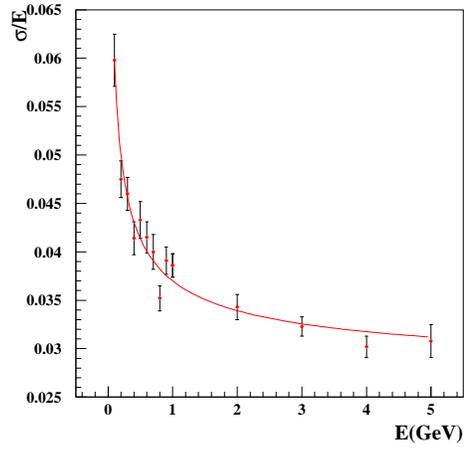
Figure 6: Energy resolution (σ/E) of forward going electrons which start at the front of the inner detector.
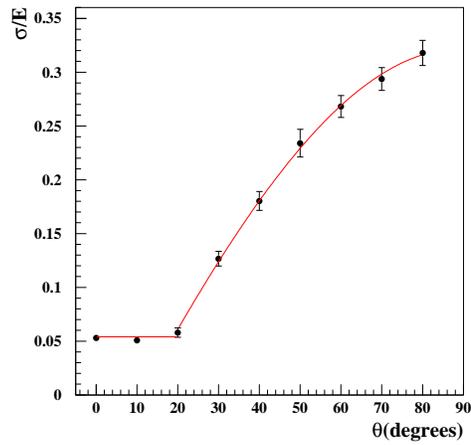

Figure 7: Energy resolution (σ/E) of 1 GeV electrons as a function of the angle the electron makes with respect to the detector axis.

π^0 **reconstruction** With the surrounding ECALs for containment, MINERνA's π^0 reconstruction capabilities are excellent. This is essential, since π^0 are a major source of background for ν_e appearance oscillation experiments. MINERνA's low density and high granularity make it an excellent photon tracker, able to accurately reconstruct the vertex and kinematics even for coherently-produced π^0's with no accompanying charged tracks.

Muons Energetic muons can be identified by their penetration of material in the calorimeters and/or MINOS near detector. Muons with a momentum measurement in the magnetic field, or which stop inside the detector can be distinguished from protons and kaons by dE/dx. In addition, the delayed $\mu \to e$ decay signature can be detected.

Charged hadrons Hadrons can be identified as such by their interactions in the inner detector and/or hadron calorimeters. Hadrons which stop without interacting or have their momentum measured by the magnetic field can also be distinguished as π, K or p with good efficiency using dE/dx. For studies of single pion and resonance production the ability to reconstruct pion and proton energies and directions is particularly important for full kinematic reconstruction. As discussed in Section 2.2, the resolution in invariant mass in the region around the $\Delta(1232)$ is around 100 MeV and the Q^2 resolution is slightly better than 0.2 $(\text{GeV/c})^2$.

dE/dx analysis Specific energy loss (dE/dx) will be an important tool for particle identification in MINERνA. For tracks which stop in the inner detector, the charge deposited near the end of the track (corrected for sample length) can be compared with expected curves for, *e.g.,* the $\pi^\pm$, $K^\pm$ and proton hypotheses. This technique does not require an independent momentum measurement, since the range (x_{stop}, in g/cm^2) from the stopping point to a given sampling point is closely correlated with the momentum at the sampling point. The algorithm is calibrated by fitting the expected dE/dx vs. x_{stop}, and the standard deviation of this quantity, $\sigma_{dE/dx}$, as a function of x_{stop} for the three different particle types (see Figure 8). The measured dE/dx for a track is compared to the expected value at each sample, to form χ^2 estimators reflecting the goodness of fit to each of the three particle identification hypotheses:

$$\chi^2(\alpha) = \sum_{i=1}^{N_{sample}} \left[\frac{\left(\frac{dE}{dx}\right)_i^{obs} - \left(\frac{dE_\alpha}{dx}\right)_i^{exp}}{\sigma_i^\alpha} \right]^2 ,$$

where the sum runs over all measured samples, and $\alpha = \{\pi, K, p\}$. The hypothesis α with the minimum χ^2 is assigned to the track. The frequency of misidentification can be visualized most easily by plotting the difference $\Delta\chi^2$ between the correct χ^2 (for the particle's true type) and the smallest of the two (incorrect) others (Figure 9). With this naïve dE/dx analysis, MINERνA correctly identifies 85% of stopping kaons, 90% of stopping pions, and $> 95\%$ of stopping protons. A similar analysis can be applied to tracks with momenta measured in the magnetic regions of the detector.
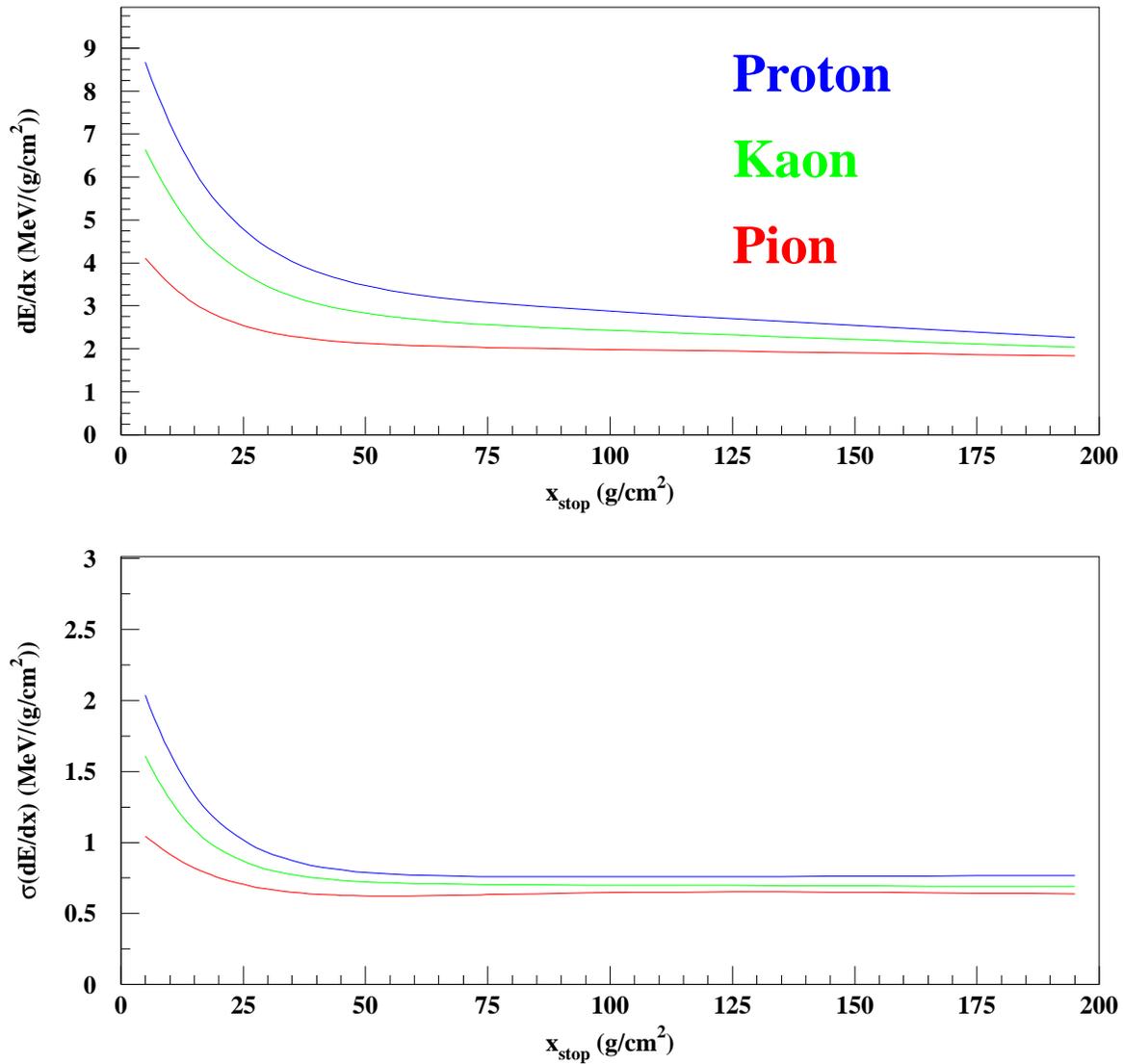
Figure 8: The top figure shows the average specific energy loss dE/dx for stopping $\pi^{\pm}$, kaons and protons, vs. range from the stopping point (in g/cm^2), for the simulated MINERνA inner detector. The bottom figure shows the estimated standard deviation of the energy loss, which is used to form a χ^2 estimator for particle identification.
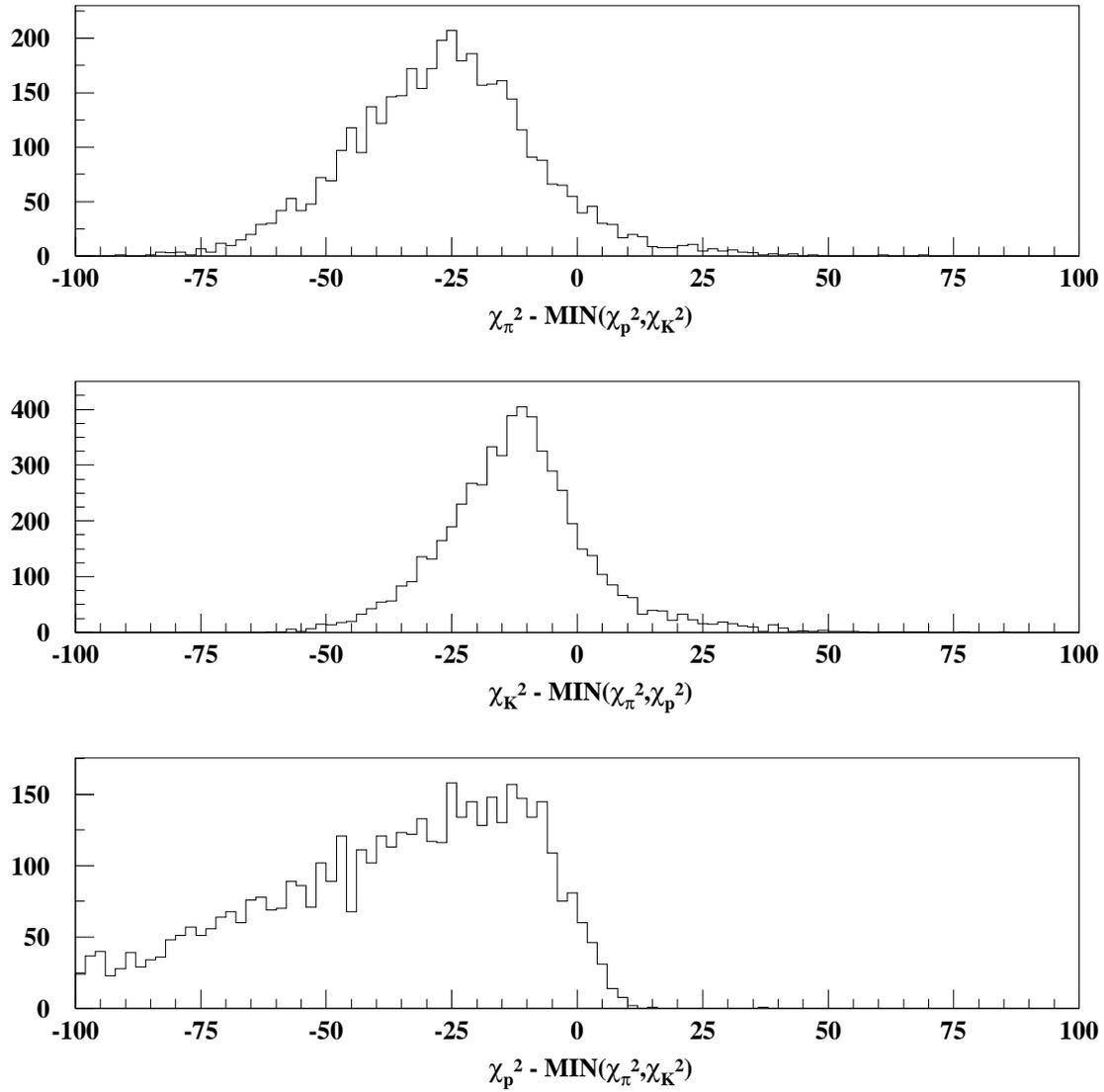
Figure 9: The three plots show the $\Delta\chi^2 \, dE/dx$ estimator for simulated and reconstructed charged pions(top), kaons(middle) and protons(bottom) stopping in the inner detector. Tracks with $\Delta\chi^2 < 0$ are correctly identified.

6.3.6 Energy reconstruction and containment

Muons The energy of muons from charged-current interactions will be measured using range and/or curvature in the magnetized regions of MINERνA and the MINOS spectrometer. For muons stopping in the detector, the momentum resolution will be $\frac{\Delta p}{p} \sim 5\%$. If the MINOS detector is used, the momentum resolution will be 13%[1].

Hadronic calorimetry Containment of hadronic energy is a significant design consideration, as it assists in meeting many of the experiment's physics goals. Studies show that the visible hadronic component of quasi-elastic and resonant events in the fully-active central region of the detector are completely contained, apart from secondary neutrinos and low-energy neutrons. Figure 10 shows the fraction of escaping visible hadronic energy for deep-inelastic reactions in several hadronic energy ranges, and figure 11 shows the probability that a deep-inelastic event will leak visible energy as a function of the true hadronic energy. Only for hadronic energies greater than 8 GeV is there any significant probability of leakage and only above 15 GeV is the average fraction of escaping energy greater than 10%. The fraction of deep-inelastic interactions with hadronic energies over 15 GeV in the low-energy, semi-medium or semi-high energy beams is $< 1\%$, and so visible energy leakage should be insignificant. These estimates ignore downstream components beyond the forward hadron calorimeter, such as the MINOS detector, and are therefore conservative.

To study MINERνA's calorimetric E_h resolution, the detector response to a neutrino sample generated throughout the inner detector by NUANCE, on carbon and hydrogen targets, was simulated. From this simulated sample, events where all hadronic fragments were contained within MINERνA were used. Hits from lepton tracks in charged-current interactions are excluded from the following analysis.

In a fully-active scintillator calorimeter, the total light yield should be essentially proportional to E_h. (The proportionality is not unity due to escaping neutrinos, rest masses of charged pions, nuclear binding energy in the initial and secondary reactions and other nuclear effects such as pion absorption.) While the central inner detector volume is fully active, there are also regions with passive iron or lead absorber sandwiched between scintillators. In these sampling calorimeter regions, not all energy deposited results in scintillation light, so the light yield is corrected accordingly.

Figure 12 shows reconstructed E_h vs. true E_h computed from the kinematics of the incoming and outgoing leptons. The relative deviation of the reconstructed energy from the true E_h, $\Delta E_h / E_h$, multiplied by $\sqrt{E_h}$ is shown in figure 12, giving a average resolution for reconstruction of E_h of $\frac{\Delta E_h}{E_h} = \frac{23\%}{\sqrt{E_h(\text{GeV})}}$. This $1/\sqrt{E_h}$ resolution has some energy dependence and is best represented by

$$\frac{\Delta E_h}{E_h} = 4\% + \frac{18\%}{\sqrt{E_h(\text{GeV})}}.$$

6.4 Event classification

Particle identification and event classification will play a central role in the analysis of data from MINERνA. One possible method of event classification is use of artificial neural network (ANN) techniques.
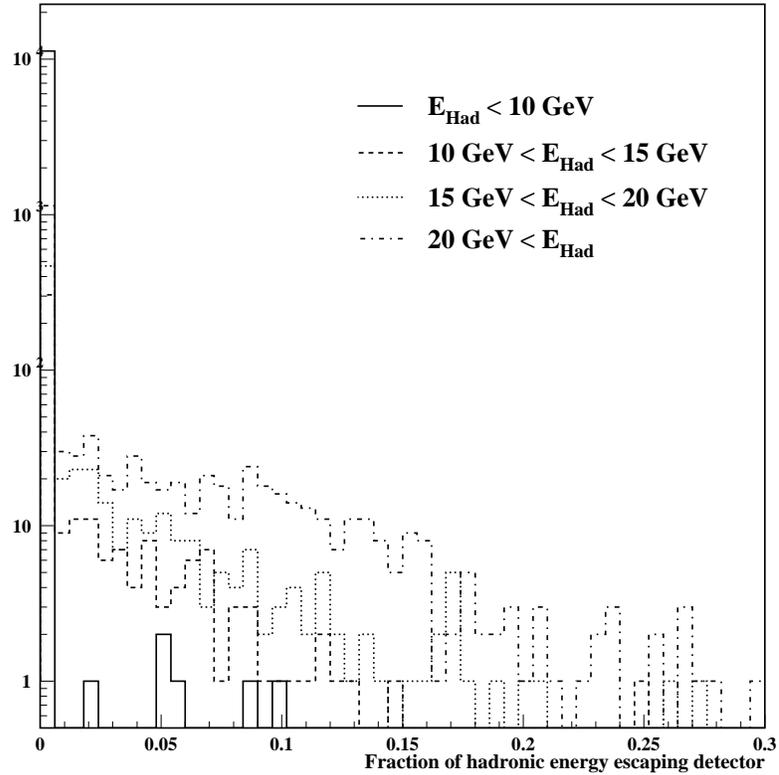
Energy Leakage for DIS events

Figure 10: Fraction of hadronic energy escaping the detector for deep-inelastic scattering in the fully-active central region.

Event classification will be based on topological characteristics as well as on particle ID. Separation of CC from NC interactions will be based on muon identification. Detection of muon decays for low energy muons stopping in the carbon gives the potential for accurate CC identification even at high y_{Bj}. In each such class further event identification will be based on other particle ID, energy/momentum measurements and kinematics. Neural networks are designed for such categorization and have been frequently used in the analysis of data from high energy physics experiments (see, for example, the DONUT[9] experiment).
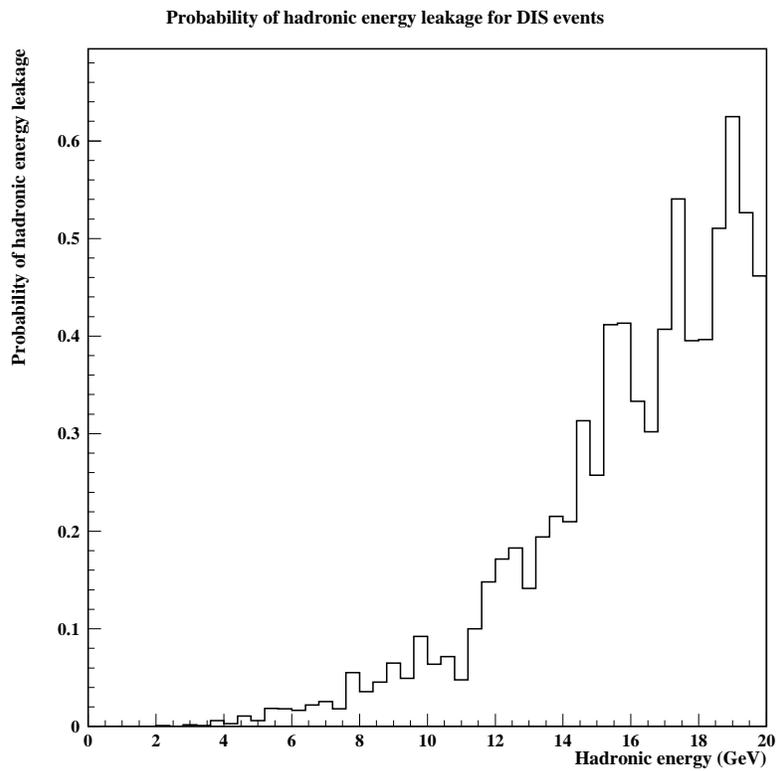
Figure 11: Probability that visible hadronic energy from a deep-inelastic event escapes undetected vs. total hadronic energy.
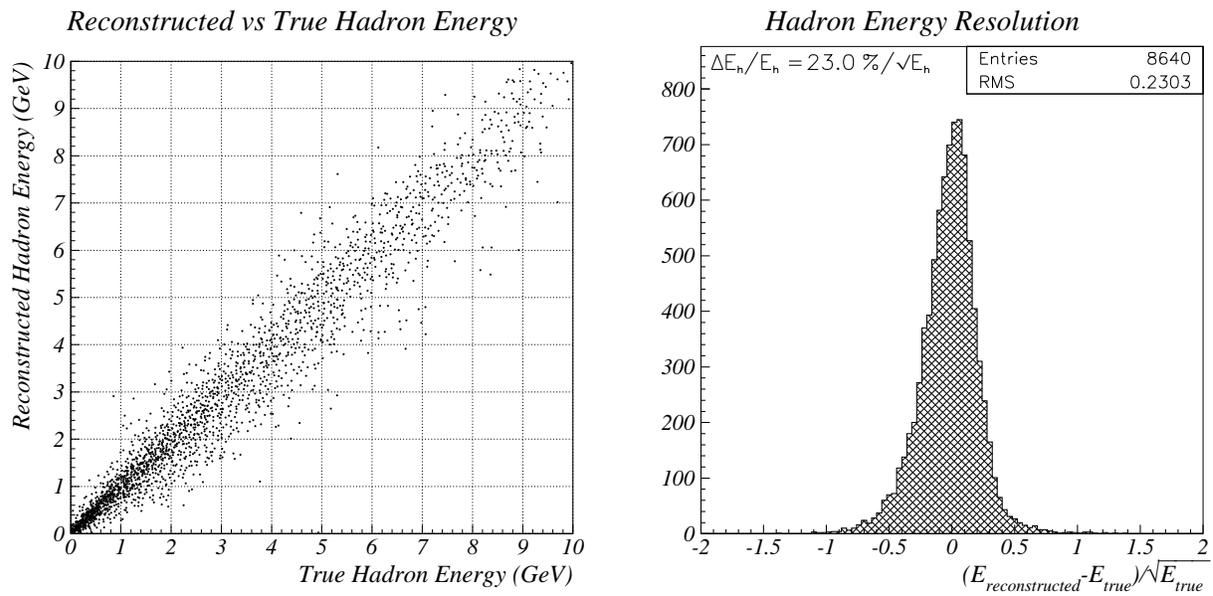
Figure 12: The left graph shows on the vertical axis the the hadronic energy E_h reconstructed from scintillator output in MINERνA vs. the true $E_h = E_\nu - E_\mu$. Right figure shows the relative deviation of the fit, $(\Delta E_h/E_h)\sqrt{E_h}$.

Part I
Bibliography

References

[1] MINOS Collaboration, "MINOS Technical Design Report", NuMI-NOTE-GEN-0337 (1998).

[2] N. V. Mokhov, "The MARS Monte Carlo", FERMILAB FN-628 (1995); N. V. Mokhov and O. E. Krivosheev, "MARS Code Status", FERMILAB-Conf-00/181 (20 00); http://www-ap.fnal.gov/MARS/.

[3] N. Mokhov and A. Van Ginneken, J. Nucl. Sci. Tech. **S1**, 172 (2000).

[4] M. Messier (private communication)

[5] Y. Hayato, To be published in *Proceedings of the Second Workshop on Neutrino-Nucleus Interactions in the Few-GeV Region (NUINT02),* Irvine, California (2002).

[6] G. Ambrosini *et al.* [NA56/SPY Collaboration], Eur. Phys. J. C **10**, 605 (1999).

[7] P-907: Proposal to Measure Particle Production in the Meson Area Using Main Injector Primary and Secondary Beams, May 2000

```
(http://ppd.fnal.gov/experiments/e907/Proposal/E907_Propsal.html
)
```

[8] NuMI Technical Design Handbook

```
(http://www-numi.fnal.gov/numiwork/tdh/tdh_index.html)
```

[9] K. Kodama *et al.*, Nucl. Phys. Proc. Suppl **98**, 43-47 (2001)

[10] M. Hasegawa *et al.* [K2K Collaboration], Phys. Rev. Lett. **95**, 252301 (2005) [arXiv:hep-ex/0506008].

[11] S. Kopp, Z. Pavlovic, and D. Indurthy, "Systematic Uncertainties in the NuMI Beam Flux" MINOS-doc-1283, (2006)

[12] C.H. Llewellyn Smith, Phys. Rep. 3C (1972).

[13] J. Arrington, nucl-ex[0305009].

[14] M. K. Jones *et al.*, Phys. Rev. Lett, 84, (2000) 1398 ; O. Gayou *et al.*, Phys. Rev. Lett, 88 (2002) 092301.

[15] J.J. Kelly, Phys. Rev. C70 (2004) 068202.

[16] R. Bradford, et al., hep[ex0602017].

[17] H. Budd, A. Bodek and J. Arrington, hep-ex[0308005].

[18] R. F. Wagenbrunn *et al.*, hep-ph[0212190].

[19] R. C. Merenyi *et al.*, Phys. Rev. D 45, 743 (1992)

[20] V. Bernard, L. Elouadrhiri, U.G. Meissner, J.Phys.G28 (2002), hep-ph[0107088].

[21] G. Zeller, private communication.

[22] K. Tsushima, Hungchong Kim, K. Saito, hep-ph[0307013].

[23] T. Kitagaki *et al.*, Phys. Rev. D26 (1983) 436.

[24] T. Kitagaki *et al.*, Phys. Rev. D42 (1990) 1331.

[25] S.J. Barish *et al.*, Phys. Rev. D16 (1977) 3103.
      BNL D2

[26] N.J. Baker *et al.*, Phys. Rev. D23 (1981) 2499.

[27] W.A. Mann *et al.*, Phys. Rev. Lett. 31 (1973) 844.

[28] J. Brunner *et al.*, Z. Phys. C45 (1990) 551.

[29] M. Pohl *et al.*, Lett. Nuovo Cimento 26 (1979) 332.

[30] D. Allasia *et al.* Nucl. Phys. B **343** (1990) 285

[31] S.V. Belikov *et al.*, Z. Phys. A320 (1985) 625.

[32] S. Bonetti *et al.*, Nuovo Cimento 38 (1977) 260.

[33] K.L. Miller *et al.*, Phys. Rev. D26 (1982) 537.

[34] Glen Cowan, Statistical Data Analysis, Oxford Clarendon Press (1 998)

[35] H. Budd, A. Bodek and J. Arrington, hep-ex[0410055].

[36] D. Casper, Nucl. Phys. Proc. Suppl. 112 (2002) 161.

[37] R.A. Smith and E.J. Moniz, Nucl. Phys. B43 (1972) 605.

[38] Ghent Theory group in Belgium, Jan Ryckebusch (jan@inwpent5.UGent.be).

[39] D. Rein and L. M. Sehgal, Annals Phys. **133**, 79 (1981).

[40] M.H. Ahn, et al. (K2K), Submitted to PRD, hep-ex/0606032.

[41] T. Sato, D. Uno, and T.-S.H. Lee, Phys. Rev. **C67** 065201 (2003).

[42] E. Paschos, M. Sakuda, J.-Y. Yu, Phys. Rev. D**69** 014013 (2004).

[43] E. Paschos, et al., Proc. NuInt04 (L'Aquila), hep-ph/0408185.

[44] O. Lalakulich and E. Paschos, Phys. Rev. D**71** 074003 (2005).

[45] O. Lalakulich, E. Paschos, G. Piranishvili, Phys. Rev. D**74** 014009 (2006).

[46] T. Sato, et al., Proc. NuInt05 (Okayama),nucl-th/0601069.

[47] T. Kitagaki, et al., Phys. Rev. D**34** 2554 (1986).

[48] T. Kitagaki, et al., Phys. Rev. D**42** 1331 (1990).

[49] M. Hasegawa, et al. (K2K), Phys. Rev. Lett. **95** 252301 (2005).

[50] M. Wascko (MiniBoone), Proc. NuInt05 (Okayama), hep-ex/060 2050.

[51] D. Rein and L. M. Sehgal, Nucl. Phys. **B223**, 29 (1983).

[52] E. A. Paschos and A. V. Kartavtsev, (2003), hep-ph/0309148.

[53] Super-Kamiokande and K2K, C. Mauger, Nucl. Phys. Proc. Suppl. **112**, 146 (2002).

[54] BooNE, J. L. Raaf, Nucl. Phys. Proc. Suppl. **139**, 47 (2005), hep-ex/0408015.

[55] B. Z. Kopeliovich, Nucl. Phys. Proc. Suppl. **139**, 219 (2005), hep-ph/0409079.

[56] E. A. Paschos, A. Kartavtsev, and G. J. Gounaris, (2005), hep-ph/0512139.

[57] D. Rein and L. M. Sehgal, (2006), hep-ph/0606185.

[58] S. K. Singh, M. Sajjad Athar, and S. Ahmad, (2006), nucl-th/0601045.

[59] MiniBooNE, J. Monroe, Nucl. Phys. Proc. Suppl. **139**, 59 (2005), hep-ex/0408019.

[60] K2K, T. Ishida, Prepared for 1st Workshop on Neutrino - Nucleus Interactions in the Few GeV Region (NuInt01), Tsukuba, Japan, 13-16 Dec 2001.

[61] N.J. Baker *et al.*, Phys. Rev. D **24**, 2779 (1981).

[62] A. Alavi-Harati *et al.*, Phys. Rev. **87** 132001 (2001).

[63] P.G. Ratcliffe, Phys. Rev. **D59**, 014038 (1999).

[64] N. Cabibbo *et al.*, Semileptonic Hyperon Decay and CKM Unitarity, [arXiv:hep-ph/0307214] (July 2003).

[65] T. Alexopoulos *et al.* (KTeV Collaboration), Phys. Rev. Lett. **93**, 181802 (2004).

[66] T. Nakano *et al.*, [arXiv:hep-ex/0301020]; V.V. Barmin em et al., [arXiv:hep-ex0304040]; S. Stepanyan [arXiv:hep-ex/0307018].

[67] R. Jaffe and F. Wilczek, Di-quarks and Exotic Spectroscopy, [arXiv:hep-ph/0307341] (July 2003).

[68] S. Kuhlmann *et al.*, Phys. Lett. B **476**, 291 (2000).

[69] H. Deden and et al., [Gargamelle Neutrino Collaboration], "Experimental Study Of Structure Functions And Sum Rules In Charge Changing Interactions Of Neutrinos And Anti-Neutrinos On Nucleons," Nucl. Phys. **B85**, 269 (1975).

[70] K. Varvell *et al.* [BEBC WA59 Collaboration], Z. Phys. C **36**, 1 (1987)

[71] M. Shifman, Handbook of QCD, Volume 3, 1451, World Scientific (2001)

[72] F. E. Close and N. Isgur, Phys. Lett. B **509**, 81 (2001)

[73] W. Melnitchouk, R. Ent and C. Keppel, Phys. Rept. **406**, 127 (2005) [arXiv:hep-ph/0501217].

[74] I. Niculescu *et al.*, Phys. Rev. Lett. **85**, 1186 (2000)

[75] C. E. Keppel, *Prepared for Exclusive Processes at High Momentum Transfer, Newport News, Virginia, 15-18 May 2002*

[76] J. Arrington, R. Ent, C. E. Keppel, J. Mammei and I. Niculescu, arXiv:nucl-ex/0307012 (submitted to Phys. Rev. Lett.)

[77] A. Fantoni [HERMES Collaboration], Eur. Phys. J. A **17**, 385 (2003).

[78] I. Niculescu *et al.*, Phys. Rev. Lett. **85**, 1182 (2000).

[79] A. Bodek and U. K. Yang, arXiv:hep-ex/0203009.

[80] D. Dolgov *et al.* [LHPC collaboration], Phys. Rev. D **66**, 034506 (2002) [arXiv:hep-lat/0201021].

[81] I. Niculescu, J. Arrington, R. Ent and C. E. Keppel, Phys. Rev. C **73**, 045206 (2006) [arXiv:hep-ph/0509241].

[82] X. Ji, Phys. Rev. Lett. **78**, 610 (1997).

[83] X. Ji, Phys. Rev. **D55**, 7114 (1997).

[84] A. V. Radyushkin, Phys. Lett. **B380**, 417 (1996).

[85] A. V. Radyushkin, Phys. Lett. **B385**, 333 (1996).

[86] J.C. Collins, L. Frankfurt, and M. Strikman, Phys. Rev. **D56**, 2982 (1997).

[87] A. V. Radyushkin, Nucl. Phys. **A711**, 99 (2002).

[88] M. Vanderhaeghen, Nucl. Phys. **A711**, 109 (2002).

[89] M. Diehl, hep-ph/0307382 (2003).

[90] C. Munoz Camacho, et al. nucl-ex/0607029 (2006).

[91] A. Psaker, W. Melnitchouk and A. Radyushkin, in preparation.

[92] D. Drakoulakos *et al.* [Minerva Collaboration], fine-grained detector in the NuMI beam," arXiv:hep-ex/0405002. Pgs. 99 - 108, 192 - 200.

[93] B.Z. Kopeliovich, hep-ph/0409079.

[94] M.K. Jones *et al.*, Phys. Rev. **C48**, 2800 (1993); R.D. Ransome *et al.*, Phys. Rev. **C46**, 273 (1992); R.D. Ransome *et al.*, Phys. Rev. **C45**, R509 (1992).

[95] D. Rowntree *et al.*, Phys. Rev. **C60**, 054610 (1999); B. Kotlinksi *et al.*, Eur. Phys. J. **A9**, 537 (2000).

[96] E. A. Paschos, M. Sakuda, I. Schienbein and J. Y. Yu, arXiv:hep-ph/0408185.

[97] M. Arneodo, Phys. Rept. **240**, 301 (1994).

[98] G. Piller and W. Weise, Phys. Rept. **330**, 1 (2000).

[99] B. L. Ioffe, V. A. Khoze, and L. N. Lipatov, *Hard processes: Phenomenology, Quark-Parton Model* (Elsevier Science Publishers, North Holland, 1984).

[100] G.B. West, Ann. Phys. **74** (1972) 464.

[101] S. V. Akulinichev, S. A. Kulagin, and G. M. Vagradov, Phys. Lett. B **158**, 485 (1985); S. V. Akulinichev, S. Shlomo, S. A. Kulagin, and G. M. Vagradov, Phys. Rev. Lett. **55**, 2239 (1985).

[102] S. A. Kulagin, Nucl. Phys. A **500**, 653 (1989).

[103] C. Ciofi degli Atti and S. Liuti, Phys. Rev. C **41**, 1100 (1990).

[104] F. Gross and S. Liuti, Phys. Rev. C **45**, 1374 (1992).

[105] S. A. Kulagin, G. Piller and W. Weise, Phys. Rev. C **50**, 1154 (1994).

[106] S. A. Kulagin, W. Melnitchouk, G. Piller, and W. Weise, Phys. Rev. C **52**, 932 (1995).

[107] S. A. Kulagin, Nucl. Phys. A **A 640**, 435 (1998).

[108] W. Melnitchouk, A. W. Schreiber and A. W. Thomas, Phys. Rev. D **49**, 1183 (1994).

[109] J. Gomez, *et al.,* Phys. Rev. D **49**, 4348 (1994).

[110] S. I. Alekhin, S. A. Kulagin and S. Liuti, Phys Rev. D **69**, 114009 (2004).

[111] S. A. Kulagin and R. Petti, paper in preparation.

[112] T. H. Bauer, R. D. Spital, D. R. Yennie and F. M. Pipkin, Rev. Mod. Phys. **50**, 261 (1978) [Erratum-ibid. **51**, 407 (1979)].

[113] C. A. Pickety, and L. Stodolsky, Nucl. Phys. B **15**, 571 (1970).

[114] S. L. Adler, Phys. Rev. **135**, B963 (1964).

[115] R. J. Glauber, Phys. Rev. **100**, 242 (1955).

[116] V. N. Gribov, Sov. Phys. JETP **29**, 483 (1970) [Zh. Eksp. Teor. Fiz. **56**, 892 (1969)] ; Sov. Phys. JETP **30**, 709 (1970) [Zh. Eksp. Teor. Fiz. **57**, 1306 (1969)].

[117] B. Z. Kopeliovich, and P. Marage, Int. J. Mod. Phys. A **8**, 1513 (1993).

[118] S. A. Kulagin, arXiv:hep-ph/9812532.

[119] E. A. Paschos and L. Wolfenstein, Phys. Rev. D **7**, 91 (1973).

[120] G. P. Zeller *et al.* [NuTeV Collaboration], Phys. Rev. Lett. **88**, 091802 (2002) [Erratum-ibid. **90**, 239902 (2003)] [arXiv:hep-ex/0110059].

[121] S. A. Kulagin, Phys. Rev. D **67**, 091301 (2003) [arXiv:hep-ph/0301045].

[122] S. A. Kulagin, arXiv:hep-ph/0406220.

[123] S. A. Kulagin, arXiv:hep-ph/0409057.

[124] D. H. Lu, A.W. Thomas, and K. Tsushima, arXiv:nucl- th/0112001, K. Tsushima, H. Kim, and K. Saito, Phys. Rev. C **70**, 038501 (2004)

[125] J.J. Aubert et al., Phys. Lett. **123B**, 275 (1983); D.F. Geesaman, K. Saito, and A.W. Thomas, Annu. Rev. Nucl. Part. Sci. **45**, 337 (1995).

[126] B. Buck and S.M. Perez, Phys. Rev. Lett. **50**, 1975 (1983).

[127] S. Dieterich, et al., Phys. Lett. B **500**, 47 (2001), S. Strauch et al., Phys. Rev. Lett. **91**, 052301 (2003).

[128] JLab experiment E3-104, co-spokespersons R. Ent, R. Ransome, S. Struach, P. Ulmer. `http://www.jlab.org/exp_prog/proposals/03/PR03-104.ps`

[129] C.H.Q. Ingram, Nucl. Phys. A **684**, 122 (2001).

[130] M. K. Jones *et al.*, Phys. Rev. C **48**, 2800 (1993).

[131] M. Nakahata *et al*, Nucl. Instrum. Meth. **A421**, 113 (1 999); E. Blaufuss *et al*, Nucl. Instrum. Meth. **A458** 638 (2001).

[132] M. Diwan and J. Nelson, NuMI-NOTE-STEEL-0639 (2000)

[133] PhD Thesis of C. Smith, University College London, London, 2002 *Calibration of the MINOS Detectors and Extraction of Neutrino Oscillation Parameters*; PhD Thesis of R. Nichol, University College London, London, 2003 *Calibration of the MINOS Detectors*

[134] PhD thesis of M. A. Kordosky, University of Texas at Austin, August 2004 *Hadronic Interactions in the MINOS Detectors*

[135] PhD thesis of P. L. Vahle, University of Texas at Austin, August 2004 *Electromagnetic Interactions in the MINOS Detectors*

[136] E. A. Paschos, L. Pasquali and J. Y. Yu, Nucl. Phys. B **588**, 263 (2000) and E. A. Paschos, J. Y. Yu and M. Sakuda [arXiv:hep-ph/0308130].

[137] D. Ashery *et al.*, Phys. Rev. **C23**, 2173 (1981).

[138] H. Gallagher, Nucl. Phys. Proc. Suppl. **112**, 188 (2002)

[139] NuMI Fluxes courtesy of Mark Messier

[140] The simulation assumed the active material was resistive plate chambers and the absorber was particle board (hydrocarbons).

[141] G.P.Zeller, submitted to proceedings of 2nd International Workshop on Neutrino - Nucleus Interactions in the Few GeV Region (NUINT 02), Irvine, California, 12-15 Dec 2002 [hep-ex/0312061]

[142] Kamiokande Collaboration, S. Hatakeyama *et al.*, Phys. Rev. Lett. **81** (1998) 2016; Soudan-2 Collaboration, W. W. Allison *et al*, Phys. Lett. **B 449** (1999) 137; MACRO Collaboration, Ambrosio *et al*, Phys. Lett. **B434**, 451 (1998)

[143] Y. Fukuda et al., *Phys. Rev. Lett.* **81** (1998) 1158; Erratum **81** (1998) 4279, B.T. Cleveland et al., *Astrophys. J.* **496** (1998) 505. W. Hampel et al. (GALLEX Collaboration), *Phys.Lett.* **B 447** (1999) 127., J.N. Abdurashitov et al. (SAGE Collaboration), *Phys. Rev.* **C 60** (1999) 055801 [astro-ph/9907113]

[144] Q.R. Ahmad *et al.* Phys.Rev.Lett.**89** (2002) 011302 nucl-ex/0204009

[145] Y. Fukuda *et al.*, Phys.Rev.Lett.**81** (1998) 1562 [hep-ex/9807003]; M. Sanchez et al., Phys. Rev. **D 68**, 113004 (2003)

[146] KamLAND Collaboration (K. Eguchi et al.), Phys. Rev. Lett.**90** (2003) 021802 [hep-ex/0212021]

[147] K2K Collaboration (M.H. Ahn et al.), Phys.Rev.Lett.**90** (2003) 41801 [hep-ex/0212007]

[148] B. Pontecorvo and J. Exptl, Theoret. Phys. **34** 247 (1958); Z. Maki, M. Nakagawa and S. Sakata, Prog. Theor. Phys. **28**, 870 (1962).

[149] M. Maltoni *et al*, submitted to New J. Phys, [hep-ph/0405172]

[150] By CHOOZ Collaboration (M. Apollonio et al.), Phys.Lett.**B466** (1999) 415 [hep-ex/9907037]

[151] W. Grimus and L. Lavoura, Phys. Lett. **B572**, 189 (2003); A. Aranda, C.D. Carone, R.F. Lebed, Phys. Rev. **D62**, 016009 (2000).

[152] "A Long Baseline Neutrino Oscillation Experiment at Fermilab", E.Ables *et al*, FERMILAB-PROPOSAL-0875, Feb. 1995, 241pp.

[153] "NOVA: Proposal to build an Off-Axis Detector to Study $\nu_\mu \to \nu_e$ oscillations in the NuMI Beamline", I. Ambats *et al.*, FERMILAB-PROPOSAL-0929, Mar 2004.

[154] Y. Itow *et al*, "The JHF-Kamioka Neutrino Project", KEK report 2001-4, June 2001. [hep-ex/0106019]

[155] J. Nelson, "MINOS Oscillation Results", Neutrino 2006, Santa Fe, NM, June, 2006.

bibitemingram C.H.Q. Ingram, Nucl. Phys. A **684**, 122 (2001).

[156] E. Gallas & J. Li., "Polishing Optical Fibers for the D0 ICD in Run II", FNAL-TM-2062, 1998.

[157] The MINERνA Collaboration,

Proposal to perform a high-statistics neutrino scattering experiment using a fine-grained detector in the NuMI beam, Fermilab Proposal P-938, e-print hep-ex/0405002; see Sect. 16.5.2.

[158] M. Bonkowski, *Magnetic Field Measurement Results*,

MINERνA note MINERvA-doc-88-v1, (measurements of December 2004).

[159] D. Cherdack and W.A. Mann, *Magnetic Shielding Capabilities of the MINERvA PMT Box*, MINERνA note MINERvA-doc-164-v1.

[160] P. Adamson, et al., Nucl. Inst. Meth. A**492**, 325 (2002).

[161] P. Shanahan, priv. comm. (Nov., 2005).

[162] A. Cabrera, et al., NuMI-934 internal report.

[163] P. Harris (Sussex Univ.) provided excellent guidance and some pieces necessary for prototyping.

[164] "MCM II and the Trip Chip", J. Estrada, C. Garcia, B. Hoeneisen and P. Rubinov, August 2002, FERMILAB-TM-2226.

[165] MINOS Technical Design Report, Chapter 5: Scintillator detector fabrication, Fermilab Public

[166] Specification 9216.000-ES-435360. Available through the Fermilab Particle Physics Division.

[167] Specification 9216.000-ES-435361. Available through the Fermilab Particle Physics Division.

[168] R. Bradford, *Assembly Roadmap from Prototype Studies*, posted to FNAL MINERνA Docdb as document number 561.

[169] R. Flight, *Detector Assembly Drawings, as of 11/15/05*, available in MINERνA Docdb as document number 226.

[170] R. Flight, *Mapper Drawings*, available in MINERνA Docdb as document number 897.

[171] R. Flight, *Fiber Routing Update*, available in MINERνA Docdb as document number 741.

[172] D. Casper, "The nuance Neutrino Physics Simulation, and the Future", *http://nuint.ps.uci.edu/nuance/files/nuance_nuint01.pdf*

[173] O. Benhar, [arXiv:nucl-th/0307061].

[174] K. Ruddick (private communication).

[175] L. Mualem (private communication).

[176] MINOS Collaboration, P. Adamson *et al.*, IEEE Trans. Nucl. Sci. **49**, 861 (2002).

[177] R. Fruhwirth, Nucl. Inst. Meth. **A262**, 444 (1987).

[178] "Studies of Extruded Plastic Scintillator for MINOS", Karol Lang and Todd Soesby, NuMI-NOTE-L-250, Feb 1997.

[179] M. Andrews, MINERνA Hazard Assessment, MINERνA Document 310 (2006)

[180] MINERνA Project Management Plan, MINERνA Document 59 (2006)

[181] L. Mualem, *The case for using Cesium-137 on the module mapper instead of Co-60*, NuMI-L-0653 (2000)

[182] American Institute of Steel Construction, Inc., *Manual of Steel Construction, Allowable Stress Design*, Ninth Edition

[183] American National Standard ANSI/ASME B30.20, *Below-the-hook lifting devices*

[184] Gage-Babcock & Associates, Inc. *Fire Protection/Life Safety Recommendations for the Fermilab NuMI Project* (1998)

[185] Fermilab ES&H Manual, Chapter 5032.2, Guidelines for the Design, Review and Approval of Liquid Cryogenic Targets (1995)

[186] J. Livengood, Letter to G. Brown, *National Environmental Policy Act (NEPA) Determination at Fermi National Accelerator Laboratory - "Main Injector Neutrino ExpeRiment ν–A(MINERνA)"* MINERνA Document 311 (December 2, 2005)